Case studies for detecting dam seepage with electroseismic geophysics

Paul Ferguson[1], Michael du Preez[2] and Ray Merton[1]

[1] *Geo9 Pty Ltd, Sydney, Australia*

[2] *ATS Ltd, New Zealand/South Africa*

This research demonstrates the recent innovative application of electroseismic (ES) geophysics to map leakage through dam walls. A preliminary comparative study suggests that ES is as effective at mapping earthen dam wall leaks as magnetometric resistivity (MMR) survey technologies. This paper demonstrates the first steps in establishing the practical use of the ES technology as a cost effective and accurate method for detecting and monitoring water seepage from dams.

Keywords: *electro-kinetics, electroseismic, dam seepage, dams, geophysics*

Introduction

Background

The initial research which contributed to the understanding of the electroseismic (ES) effect was carried out by Frenkel (1944). He described the relative flow of fluid in a medium brought about by the passage of seismic compression waves (P-waves). Frenkel investigated the induced electric fields generated by this relative fluid–matrix motion using Helmholtz-Smoluchowski Equations (Smoluchowski 1914). However, investigations did not fully explain this relationship. Biot (1964) made further progress by developing theories that predicted movement of a seismic wave through saturated porous media.

Various advances toward deriving equations to describe the link between relative fluid-matrix interactions and the resulting electromagnetic fields were generally developed between 1962 and 1994. Haartsen and Pride (1995) built on this knowledge by clarifying aspects relating the induced electromagnetic fields, generated by dynamic current imbalances produced by plane shear waves moving across the interface between rocks with different ES properties (Haartsen and Pride 1995). The induced electromagnetic fields can be read at the surface as an interface response. If the plain shear waves pass through a homogeneous saturated medium, with no interfaces of different ES properties, then the net currents induced will be balanced, cancelling each other out. Thus no current flow is induced by the relative motion of the fluid and no electromagnetic fields can be measured at the surface.

Haartsen and Pride (1997) applied their findings to investigate ES waves from single point sources in layered rock. They determined the signal created at the interface boundary of saturated media is related to a dipole-induced field directly under the point of the seismic source. Haartsen (1998) also proved the ES response is correlated to salinity, porosity and permeability within the porous elastic media.

The electric double layer

Materials such as grains of rock display net electric charges on their surfaces due to unsatisfied chemical bonds. In an aquifer, water exhibits an electrolytic characteristic in contact with these charged surfaces producing an electric potential. This charged potential difference draws solvated ions toward the rock grain surface by Van der Waal forces forming an electric double layer (Figure 1). The inner layer is called the Stern Layer while the outer is termed the Gouy Layer, which consists of free ions in the surrounding water. The Stern Layer consists of a single ion layer with the electric potential decreasing abruptly across it. In conditions with low electrolytic concentrations (lower than 0.1 moles per litre), the electric potential in the Gouy Layer is described by Equation 1:

Equation 1. Equation for calculating electric potential in low electrolyte conditions.

$$\varphi(x) = \varphi_0 e^{-kx}$$

where:

φ = electric potential
k = inverse of the Debye radius
x = distance from the charged surface

The slipping plane is defined as the area between the solid surface and the strongly bound ions and the outer diffuse layer of ions. The slipping plane has an electric potential across it called the zeta potential (ζ), produced by the shearing between the Stern and Gouy Layers. The zeta potential partially determines the magnitude of the induced electromagnetic field.

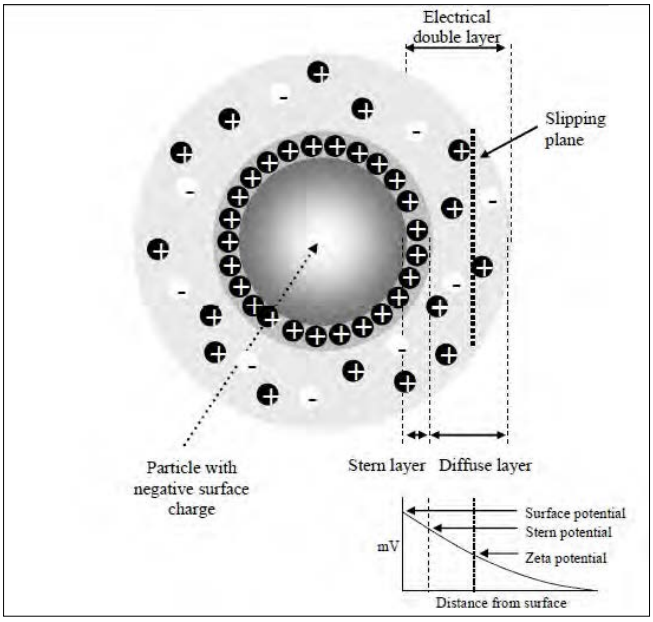

Figure 1. The electric double layer (http://www.escubed.co.uk/sites/default/files/zeta_potential_(an013)_streaming_potential.pdf)

The Electroseismic Effect

The ES effect is observable when a P-wave intersects a water saturated interface of differing inelastic or electrical characteristics. Energy is converted and dissipated when P-waves pass through an interface to form slower P-waves, which in turn produces increased relative movement between the rock and water. ES signals are produced by the out of phase motion between all the ions in the water and those attached to the rock surface.

The relationship between applied pressure P and electric potential response (φ) for a porous rock is generally given by Equation 2 (Millar and Clarke, 1997) as:

Equation 2. Relationship between incident pressure and electric potential response.

$$\varphi = -CP = -(\varepsilon\varepsilon_0\zeta/\eta\sigma)P$$

where:

φ = electrical potential response or streaming potential

C = electroseismic coefficient

P = applied pressure

εε0 = permittivity of the pore space

ζ = zeta potential

η = fluid viscosity

σ = electrical conductivity

This equation relates the electrical response induced in a porous rock from an incident P-wave stimulus allowing the rock to be characterised by the ES effect on a macroscopic scale (Fourie 2003).

Wave behaviour

There are two ES effects produced when a seismic wave propagates through a medium. The first is caused when a spherical P-wave crosses the interface between two media creating a dipole charge separation due to current imbalances (Figure 2). The second effect is caused when a seismic wave travels along an interface creating a charge separation and inducing currents on opposite sides of the interface with an associated electrical field. The electric field moves along the interface and can be detected by antennas when the head wave passes underneath (Figure 3).

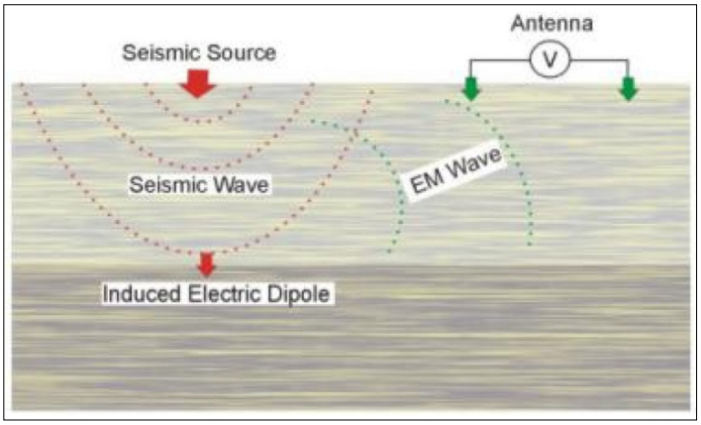

Figure 2. Seismic wave crossing an interface generating an electromagnetic wave (Anthony 2006)

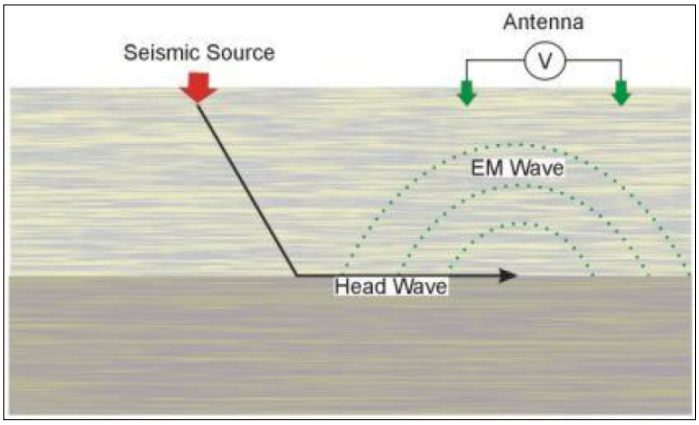

Figure 3. Head wave travelling along an interface generating an electromagnetic wave (Anthony 2006)

Method

On a planned survey grid, the survey points are navigated to with a GPS or DGPS. At each location, a seismic signal is generated by striking a hammer onto a metal plate at least 5

times. This seismic signal generates the ES effect. Generation of the seismic signal with a sledge hammer is effective in most settings to a depth between 200 – 400 m. The ES effect results in an electrical potential between the two rod electrodes (Figure 4). The rods are connected to an audio recorder by two clamps and a cable and the potential is recorded as a digital audio file. If the rods cannot be firmly positioned in the ground, sponges soaked in salt water are used instead, which is frequently the case on dam walls.

Long conductors such as metal fences, road side guards, power lines and communication cables and other cultural features are mapped so their electrical interference effects can be eliminated. The recorded signal is cleaned by filtering electrical interference using specific algorithms.

The gathered information is processed to indicate hydraulic conductivity. When there is no correlation data in the form of well logs or well pump test data, the results are described as relative values and cannot be taken as actual field values. The ES method can resolve different construction materials by their differing electrical properties. There will also be slight variances in the calibration for seismic velocities that dictate depth estimations due to the materials and make-up of the dam wall.

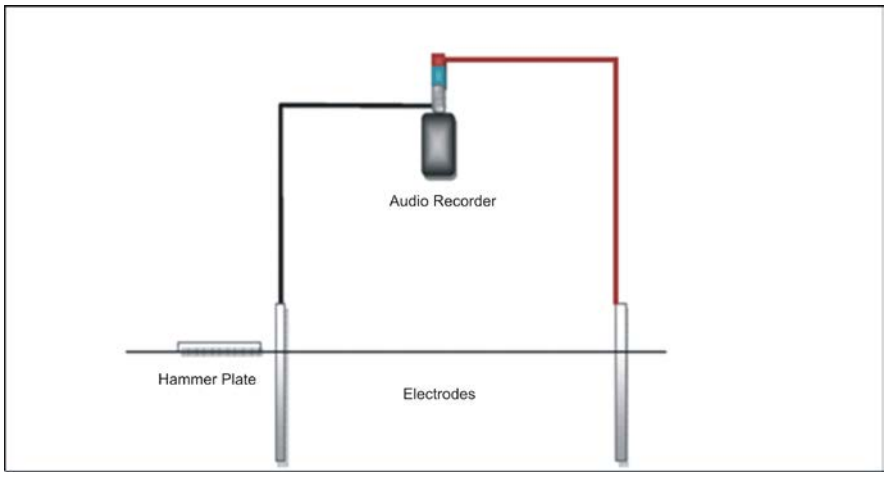

Figure 4. Basic electroseismic field equipment configuration.

Case 1 - Comparison of electroseismic and magnetometric resistivity surveys at Silvan Dam, Monbulk Earthen Dam Wall

Site description

This study was carried out on the Monbulk Dam earthen wall (Figure 5) to determine the positions and depths of potential leakage points within and under the western half of the dam wall (De Moel *et al*. 2011 for a summation of the dam's construction and foundations). The focus of this study was to compare the ES results against the magnetometric resistivity (MMR) survey results conducted by Geo9 in association with Willowstick from March 2011 (De Moel *et al*. 2011). Twenty five soundings were carried out on the upstream side of the buried concrete barrier. The distance between each was ~5 m, with their locations recorded via a Garmin eTrex10 GPS and position averaged to an error of +/- 3m (Figure 6). The results of these soundings are illustrated on Figures 7, 8, 9, 10 and 11 as one profile line. The profiles are rendered to a depth of 12 m.

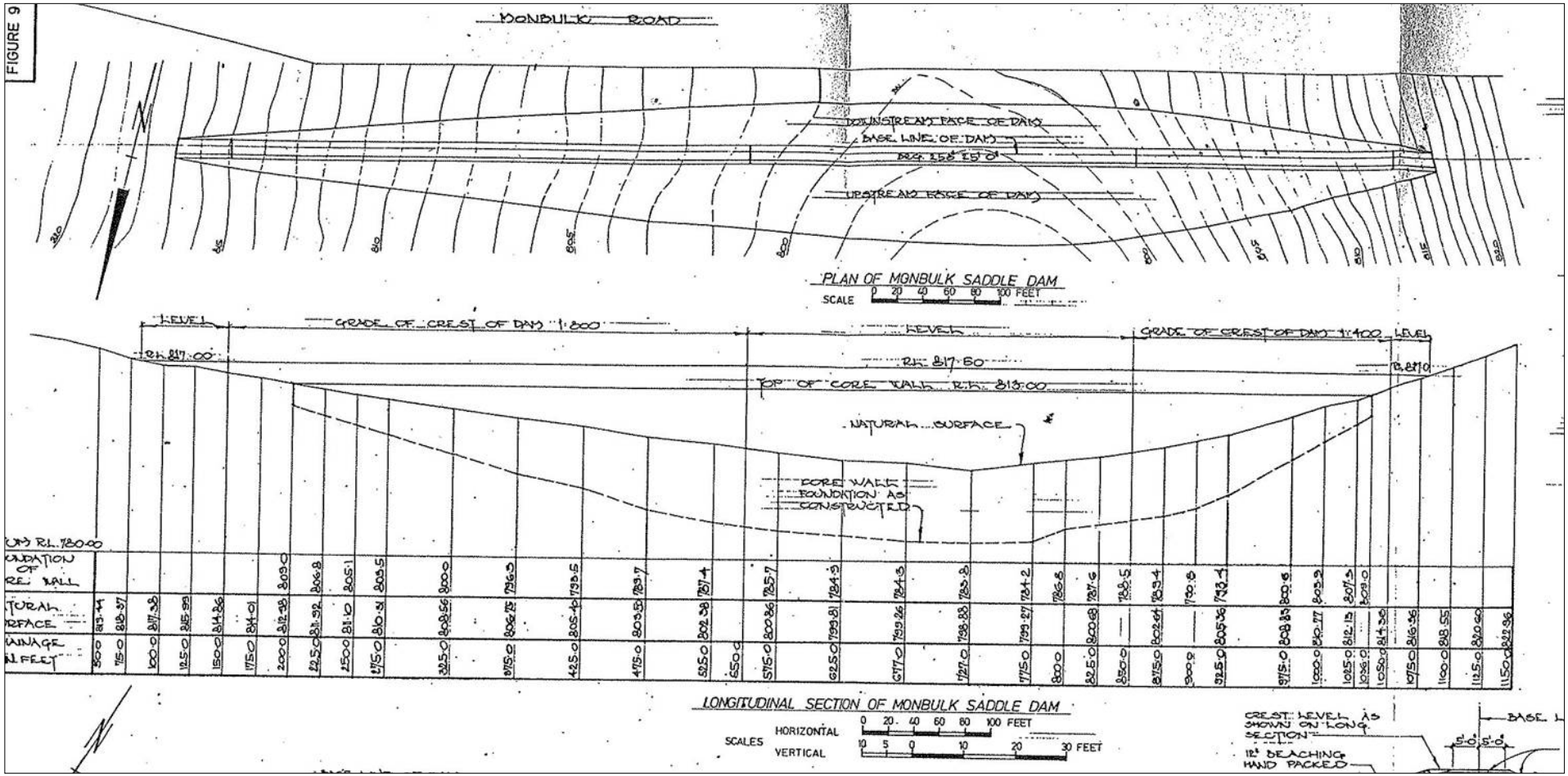

Figure 5. Silvan Dam, Monbulk saddle earthen dam wall cross section (courtesy of Melbourne Water)

Figure 6. The locations of 25 electroseismic soundings on a Google Earth image

Hydraulic conductivity tomography

The positions and direction of this profile are indicated on Figure 6, and the ES hydraulic conductivity results are shown in Figure 7. Hydraulic conductivity is a measure of permeability or the ease at which a fluid, water in this case, can flow through a porous medium. It is usually expressed as a velocity in units of metres per day under a gravitational force or hydraulic gradient. Since the data is uncalibrated, the data shown in Figure 7 is displayed in terms of relative hydraulic conductivity of 0 to 1, where a value of 1 is the highest hydraulic conductivity and 0 is the lowest.

The hydraulic conductivity data shown in Figure 7 is displayed in relation to the known natural surface level shown as a dotted line, and upstream of the concrete wall shown in transparent white. The data indicates saturated permeable formations of variable hydraulic conductivity under the concrete wall, over the majority of the survey site area. There are three locations to the west of the site that show significantly higher relative hydraulic conductivity values than the rest of the site. The data indicates there is a great deal of similar permeable formations to the east of the site as well, hinting at a larger dam leakage problem.

The data also suggests there are no significant saturated formations behind the concrete dam wall, indicating the majority of the concrete dam wall centre is sound and water tight. There is however a small anomaly at 38 m on the profile line, shown on Figure 7, indicating a possible leakage through the concrete wall at that location. This is very weak in comparison to the rest of the high permeability zones and as such, is negligible.

Electroseismic groundwater flow potential tomography

Figure 8 shows the ES groundwater flow potential indicating the areas under the site that show the highest flow rate potential. This data is primarily used to find the best location to tap a groundwater reserve. However, in the case of a dam leakage project such as this, it indicates the most likely positions of leakage flows and relative leakage flow rate. The data shown in Figure 8 is expressed in percentage probability of highest flow rate and illustrated on the plot as a colour map with a colour gradient corresponding to the legend on Figure 8. This data lines up well with the high hydraulic conductivity zones shown in Figure 7.

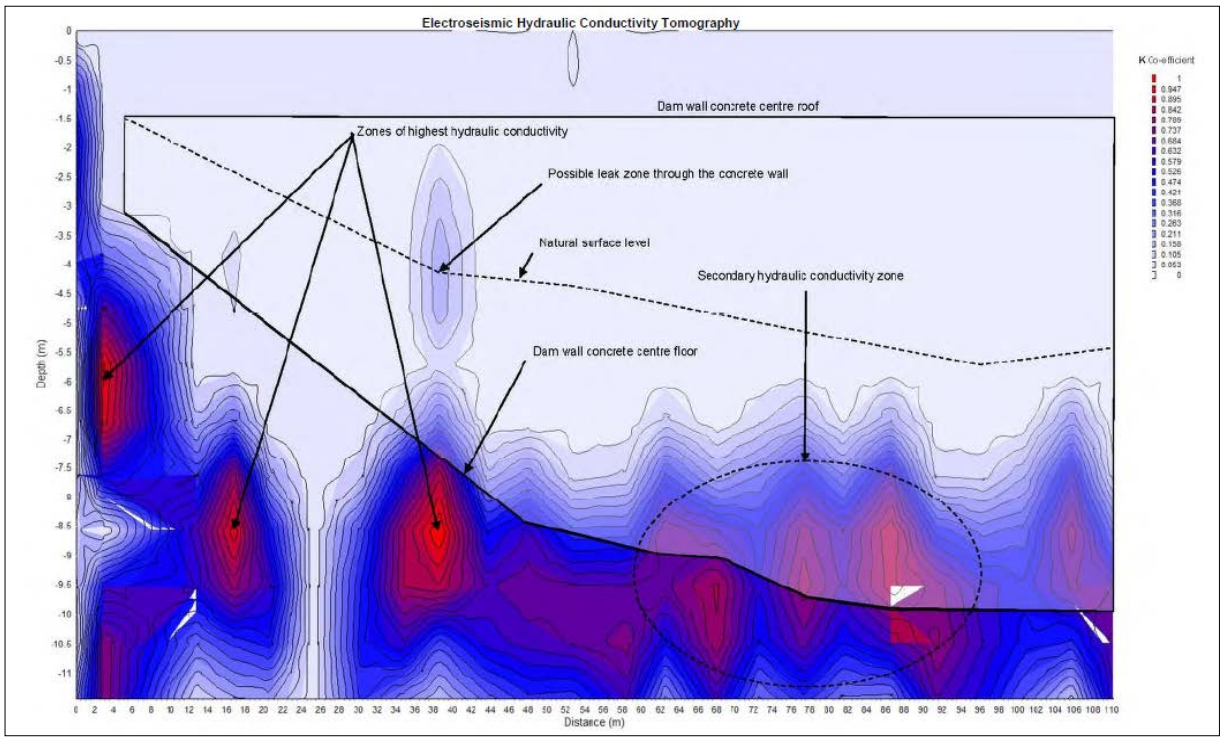

Figure 7. Electroseismic hydraulic conductivity tomography illustrates areas of higher and lower hydraulic conductivity and permeability by means of a colour contour section map, higher permeability indicated in red and very low permeability indicated in light blue (looking upstream).

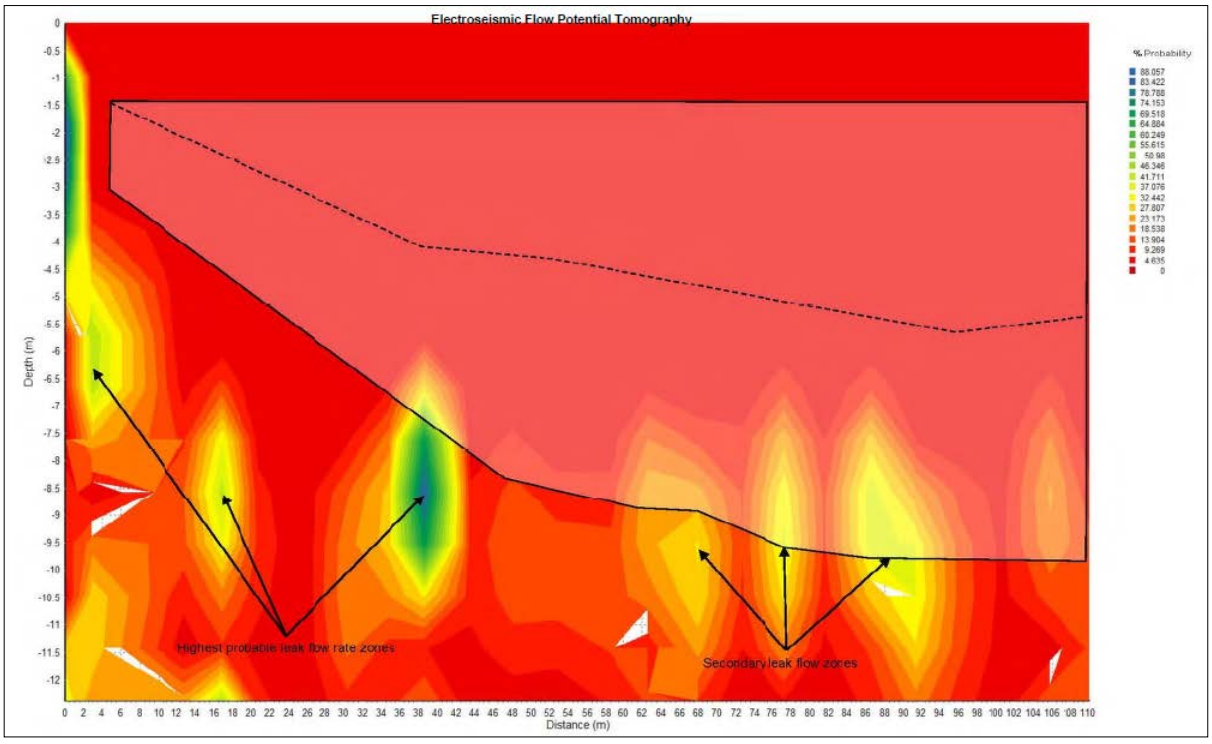

Figure 8. Electroseismic flow potential tomography expressed in percentage probability of highest flow rate and illustrated with a colour gradient corresponding (looking upstream).

Fracture analysis

Figure 9 shows the fracture analysis tomography revealing inferred fracture zone depths. The ES data is spectrally analysed and specific frequency patterns associated with fracturing are used to infer fracturing with depth. The results shown in Figure 9 are used to show secondary permeability within a primary permeability aquifer. These fractured zones are associated with higher fluid flow rates.

The direct comparison of the hydraulic conductivity data and the flow rate probability data is shown in Figure 10. This indicates the flow is of a primary permeability type and not due to cracks or fracturing within the dam wall. Figure 9 shows there is very little fracturing under the test site.

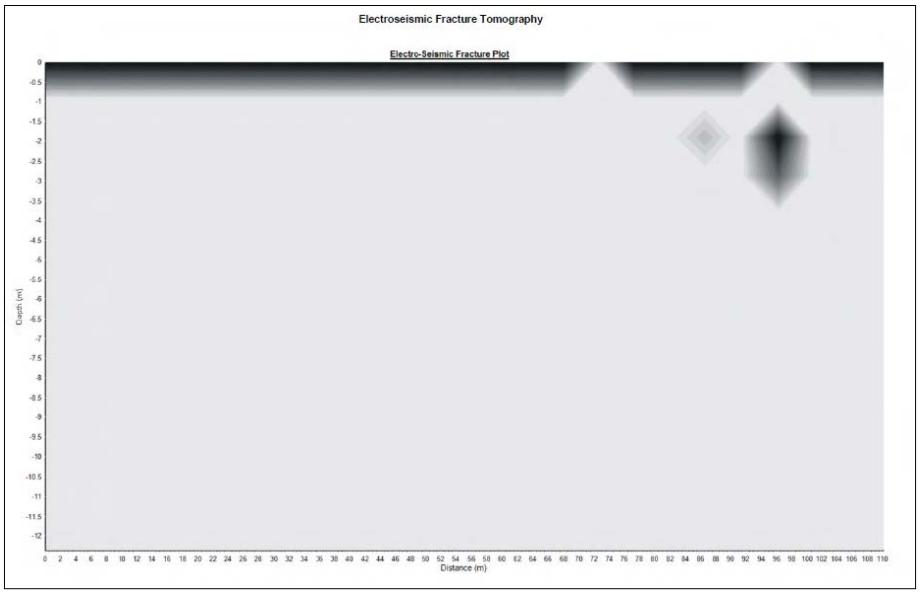

Figure 9. Electroseismic fracture tomography shows secondary permeability, i.e., fracture zones associated with a higher flow rate (looking upstream).

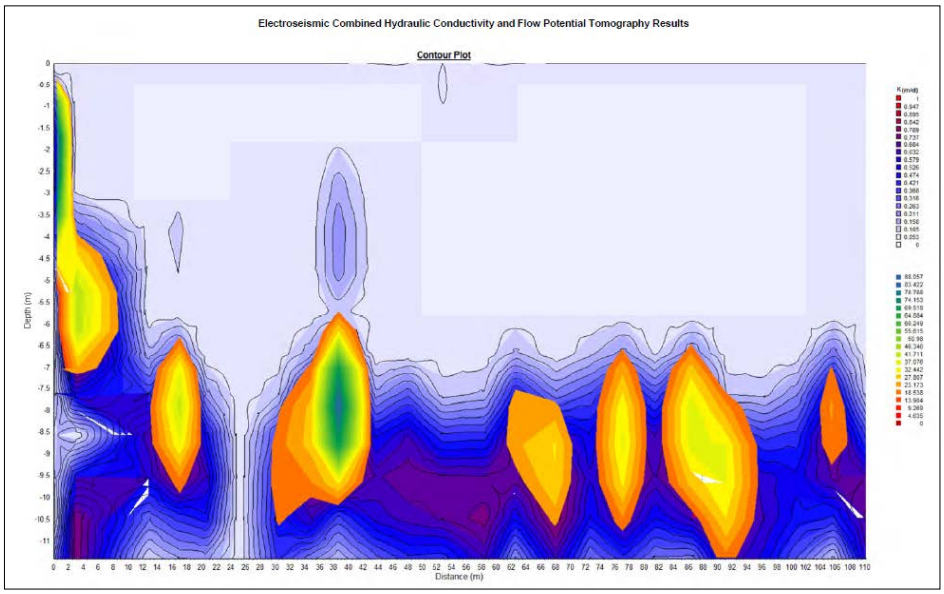

Figure 10. A direct comparison of the electroseismic combined hydraulic conductivity (Fig. 7) and flow potential tomography results (Fig. 8, looking upstream).

Case 2 - Electroseismic survey of Tailings Dam Seepage Grange Resources, Savage River Magnetite Mine, Tasmania

Site description

The data for this project was collected by Geo9 to investigate dam seepage through the tailings dam wall at Grange Resources magnetite mine at Savage River, Tasmania (Figure 11). The purpose behind the site visit was to geophysically map an ore body, and the dam survey was an opportunity to showcase the ES technology by ascertaining the positions and depths of leakage paths within and under the dam wall over a small area chosen by the client.

The Savage River mine produces high grade magnetite for smelting. The crushed waste rock is pumped as sludge into the tailings dam, which is constructed from waste rock that is a by-product of the mining process. The waste rock sludge that is held by the tailings dam has a sulphide component and measures are taken to monitor the waters pH draining from the dam. Carbonaceous rocks are incorporated into the sludge to neutralise the sulphuric acid produced from degradation of the sulphides.

The dam has had its wall height raised several times over the years as production commenced at the site in the late 1950's / early 1960's. A site adjacent to the spillway was chosen by company engineers to map the subsurface behind a known seepage area. The locations of the 26 ES soundings recorded are shown in Figure 12. Results of these soundings are illustrated in Figures 13 and 14 as one profile line. The profiles are rendered to a depth of 15m. As there was no hydrological data to calibrate the ES data against, the values are relative to each other and are not to be considered as actual values.

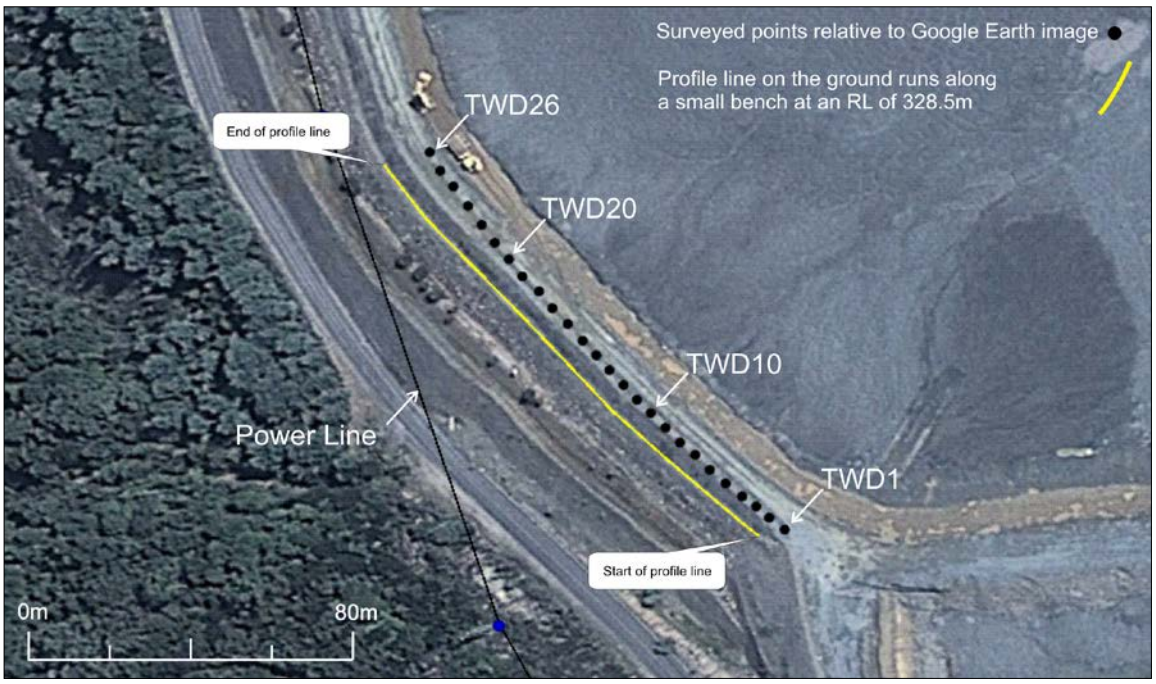

Figure 12. Electroseismic sounding profile position.

Hydraulic conductivity tomography

Figure 13 shows the profile for the ES hydraulic conductivity tomography results for the test site. As in the previous example (Figure 7), the hydraulic conductivity values shown in Figure 13 are displayed in relative terms, where a value of 1 is the highest hydraulic conductivity and 0 is the lowest.

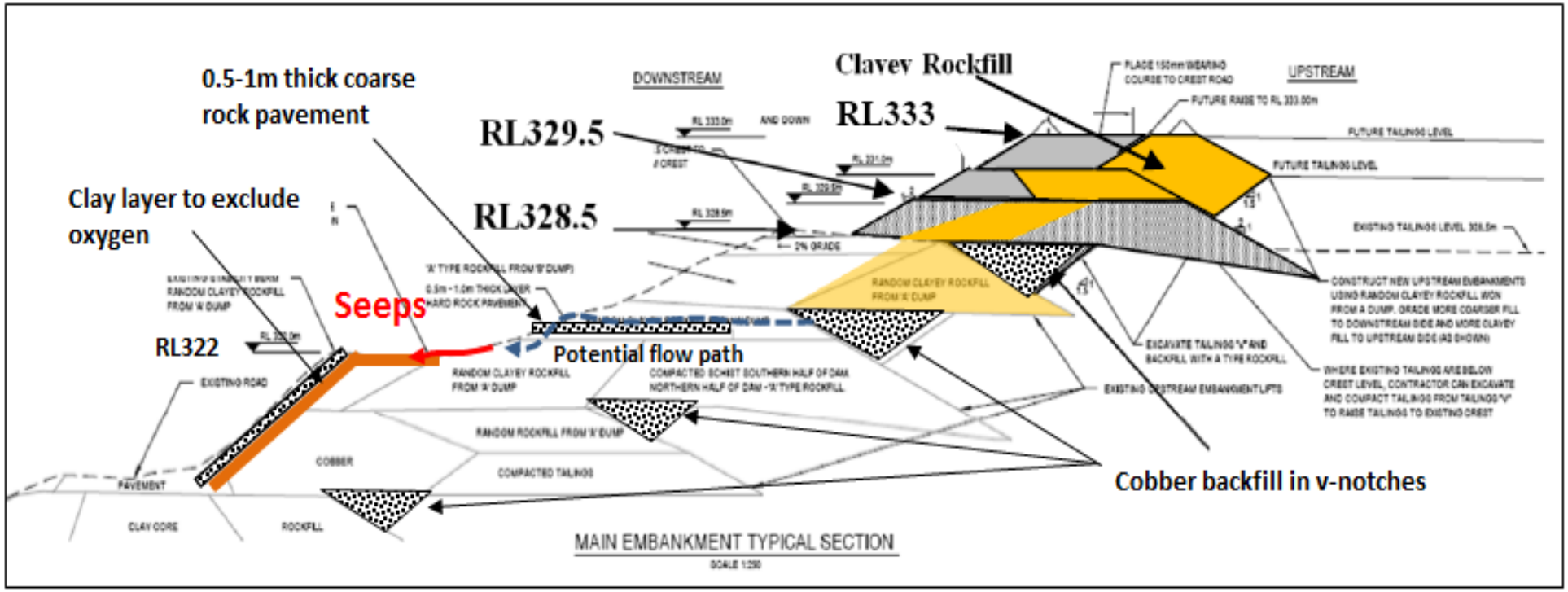

Figure 11. The up to date tailings dam wall cross section, as built (courtesy of Grange Resources)

The colour gradient in Figure 13 illustrates areas of higher and lower hydraulic conductivity and permeability under the survey site. Figure 13 indicates two distinct areas within the dam wall with higher permeability than others. These two areas are located at approximately 5 metres depth below the surface along the 328.5m RL level (Figure 11). The data also indicates low permeability outside of these two higher permeability zones, indicating the remainder of the dam wall is sound.

Electroseismic groundwater flow potential tomography

Figure 14 is the ES groundwater flow potential tomography profile indicating the most likely positions of leakage flows and relative leakage flow rate. The data shown in Figure 14 is expressed in percentage probability of highest flow rate and illustrated on the plot as a colour map with a gradient corresponding to the legend on the figure.

Figure 14 indicates the zones of highest groundwater flow probability. This data lines up well with the high hydraulic conductivity zones shown in Figure 13. There is a distinct high flow zone at 30m from the beginning of the profile line and a lower flow zone at 90m from the beginning of the line. These indicate that further investigation of these two areas should be conducted.

Discussion

This study is the first deployment of ES surveying to identify and map dam wall leakage. This has been carried out at two dam walls, specifically a water storage and a tailings dam, with different materials used in their construction. Importantly it is the first comparative study between the ES and MMR techniques already established as an effective way to map seepage paths through dam walls.

The Monbulk dam wall site was specifically targeted because a few years earlier, Geo9 had completed a MMR survey for the site (De Moel *et al*. 2011). Figure 15 shows a comparison between the hydraulic conductivity data, the flow probability data and the MMR survey data for the site. There is significant correlation between the ES data and the MMR data validating the earlier conclusion that leakage was through permeable clays in the dam foundation. It is important to note the ES method has detected other permeable zones not detected by the MMR method. It should be acknowledged this flow may have initiated in the time period between the two surveys. Importantly as yet there has been no correlation between the data presented here and the MMR data and any physical investigation or remediation work.

A more extensive data collection program at the Savage River tailings dam is planned. The majority of the dam leakage was shown to result from previously unidentified flow within the dam wall. The strategy is to acquire ES data along the same line for the whole dam wall and to be more specific over areas of concern. Seepage locations and areas will be mapped on the cross-section, and a grid of ES soundings will be collected to produce 3D models of the seepage paths. The program will include soundings at piezometers in the dam wall to enable calibration of the ES data to provide quantitative flow rates within the permeable zones. When the hydraulic conductivities are measured and flow rates calibrated the results will enable the effective planning of remediation work and/or the establishment of a monitoring regime.

This paper summarises the first steps in demonstrating the practical use of the ES technology as a cost effective and accurate method for detecting and monitoring seepage through dams. It is to be made clear that without calibration data the real permeability values are not know and since the values presented are relative, then the flow through the dam wall could be low as the data provides relative measurements only. However, the data can easily be linearly calibrated to a known hydraulic conductivity at any sounding point at any depth on the profile line. Future surveys would benefit from direct measurement of the hydraulic conductivity to enable calibrated flow rates to be estimated through the permeable areas.

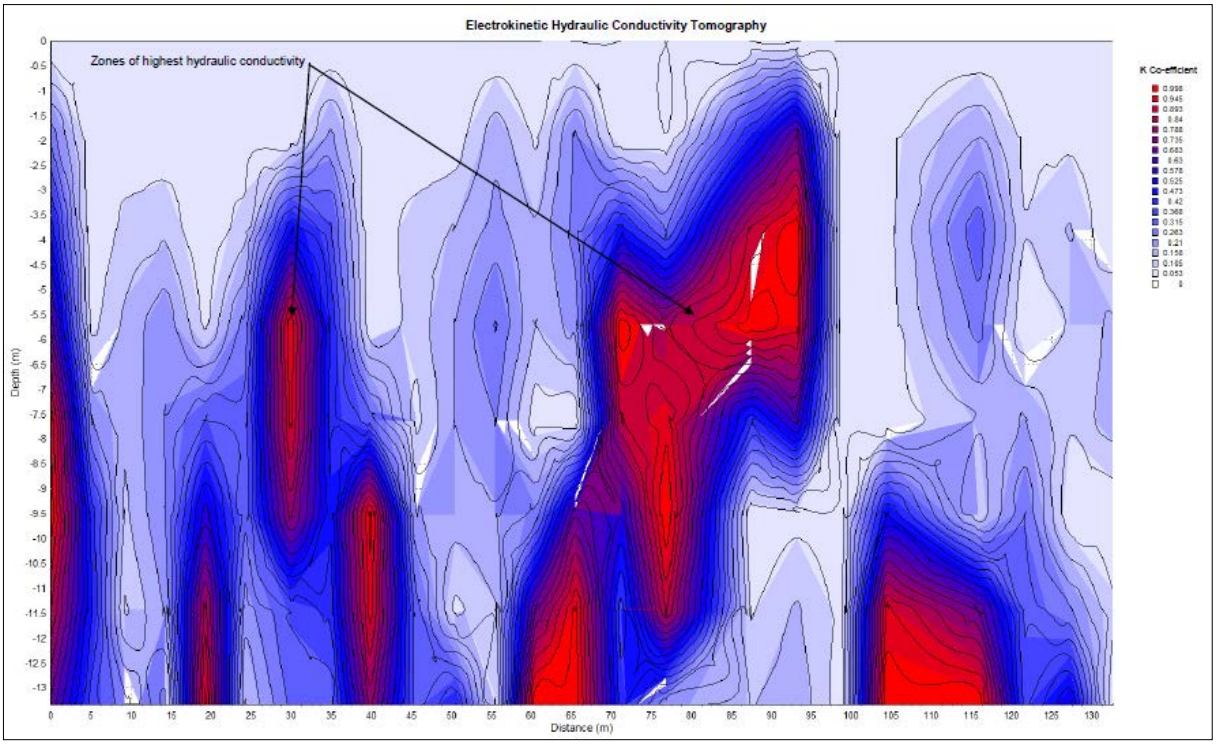

Figure 13. Electroseismic hydraulic conductivity tomography for the tailings dam at Savage River. Note: red indicates higher permeability and light blue indicates very low permeability (looking upstream).

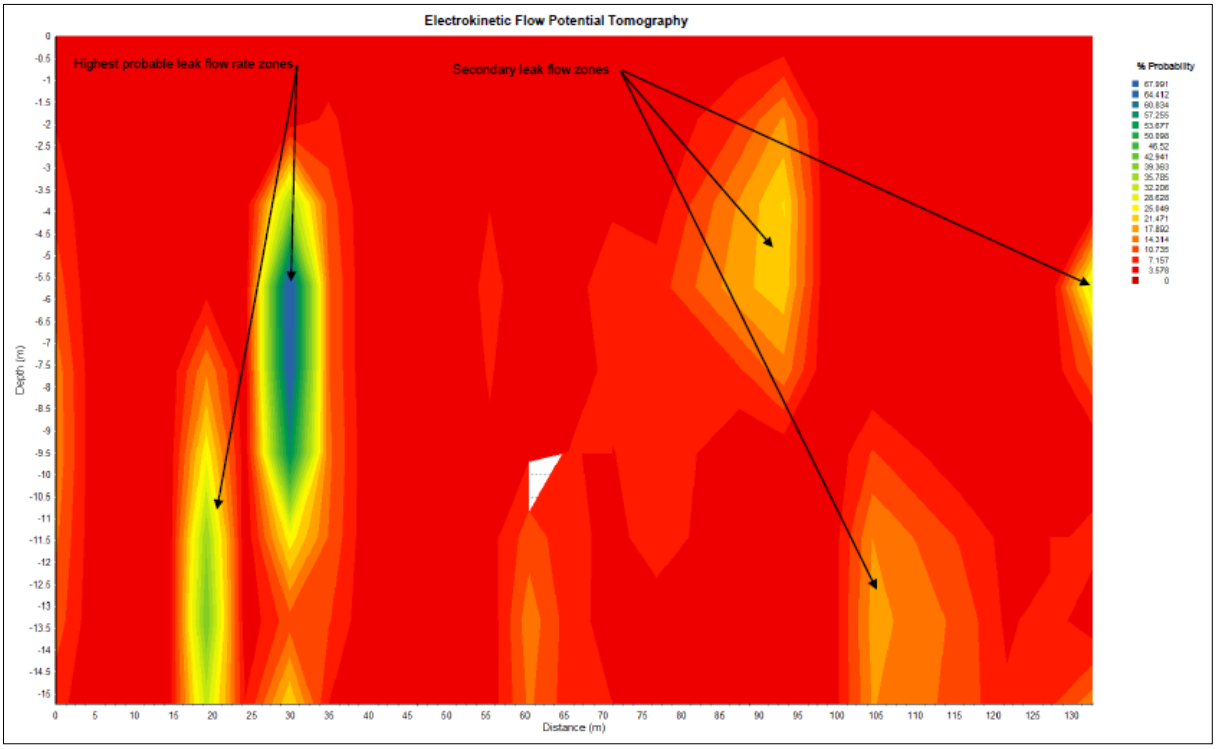

Figure 14. Electroseismic flow potential tomography for the tailings dam wall at Savage River (looking upstream).

A difficulty with including hydrogeological data relates to changing flow rates within the permeable zones resulting from changes with the dam water levels also changing the hydraulic gradients across dam walls. Importantly, the MMR survey at the Monbulk dam wall was undertaken with high dam water levels in order to increase the rate of leakage to increase mapping accuracy. It should be noted that under low dam water levels with minimum hydraulic gradient conditions the ES data returned similar mapping accuracies to that of the MMR survey under optimal conditions.

The authors plan to conduct further studies and map in 3D, leakage paths and geotechnical information within and beneath other dam types including concrete dams, ballast of varying sizes and on the water upstream of the dam walls. An example of the typical 3D modelling of hydraulic conductivity this ES technology can provide is depicted in Figure 16. This is an example from data acquired for a groundwater exploration program on a sheep and wheat farm, north of the Stirling Ranges in southern Western Australia. Geo9 has successfully demonstrated the ability of the ES to be a cost effective technique for exploring for groundwater, with results verified by drilling. ES data is integrated into modelling and visualisation software. Although beyond the scope of the study to date, there is vast potential for this technology to be applied to dam sites where change in leakage flow over time will provide an invaluable perspective to complement and guide other seepage investigation techniques, for dam safety monitoring and long term maintenance strategies of dam structures.

References

Anthony, E. 2006. Groundwater Exploration and Management using Geophysics: Northern Region of Ghana, PhD thesis, Brandenburg Technical University of Cottbus

Biot, M. A. 1964. Theory of Buckling of a Porous Slab and its Thermoelastic Analogy. *Journal of Applied Mechanics 27*, 194-198.

De Moel, M.; Arnold, M.; Adikari, G. 2011. Investigating the Piping Risk Associated with Seepage at Monbulk Saddle Dam of Silvan Reservoir, Victoria., Australian National Committee On Large Dams (Ancold) Annual Conference, Melbourne, Australia October 2011.

Du Preez, M. 2005. Accuracy of Electro-Seismic Techniques Applied to Groundwater Investigations in Karoo Formations. MSc thesis: University of the Free State

Fourie, F.D. 2003. Application of Electroseismic Techniques to Geohydrological Investigations in Karoo Rocks, PhD thesis, University of the Free State, Bloemfontein, South Africa.

Frenkel, J. 1944. On the Theory of Seismic and Seismoelectric Phenomena in Moist Soil. *Journal of Physics 8*, 230-241.

Haartsen, M. W.; Pride, S.R. 1995. Modelling of Coupled Electroseismic Waves from Point Sources in Layered Media, Journal of Geophysical Research

Haartsen, M. W.; Pride, S.R. 1997. Electroseismic Waves from Point Sources in Layered Media. Journal of Geophysical Research.

Millar, J.W.A.; Clarke, R.H. 1997. Electrokinetic Techniques for Hydrogeological Site Investigations, Groundflow.

Smoluchowski, M. 1914. Handbuch der Elecktrizitat und des Magnetismus, L. Graets, *ed*., Vol. 2, J.A. Barth, Leipzig.

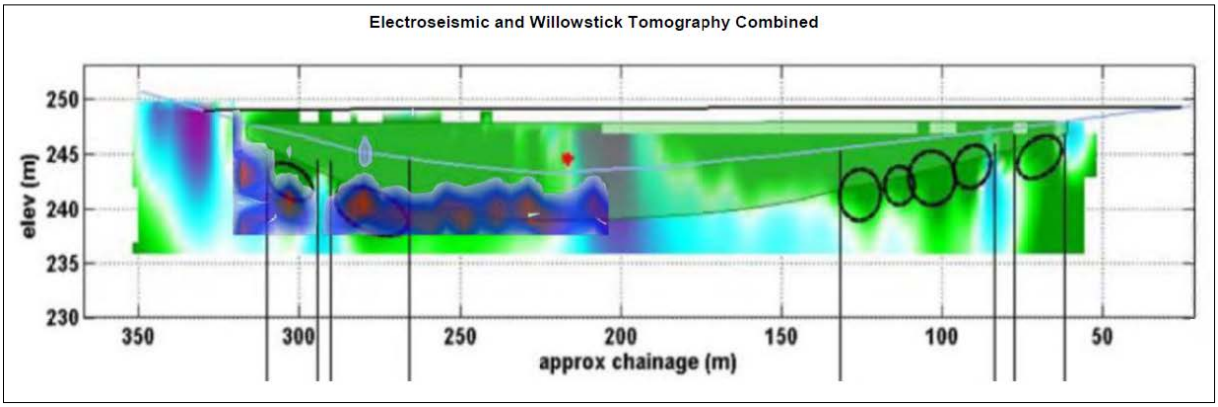

Figure 15a. Electroseismic hydraulic conductivity combined with the magnetometric resistivity results

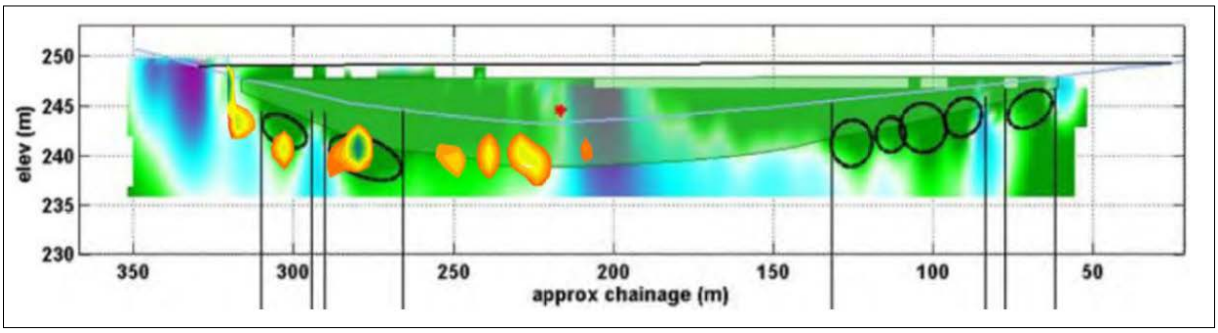

Figure 15b. Electroseismic flow potential combined with the magnetometric resistivity results

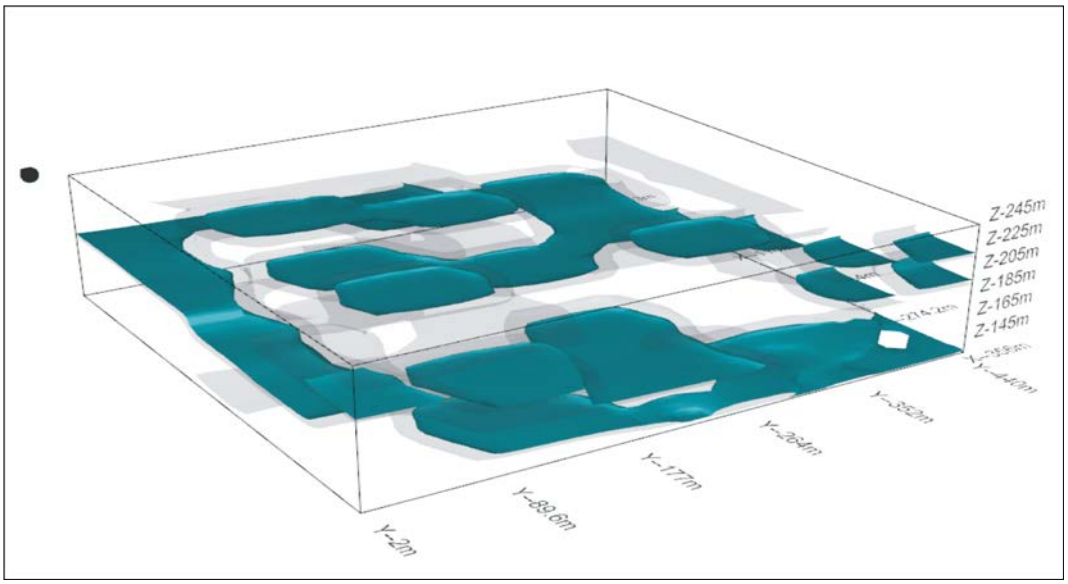

Figure 16. 3D groundwater exploration results. This model is for a 500m x 500m area, with two iso-surfaces of 0.8 (blue) and 0.5 (light grey) coefficients expressing important relative hydraulic conductivity spatial variability.